International Journal of Thermal Sciences 49 (2010) 721–732

Contents lists available at ScienceDirect

International Journal of Thermal Sciences

journal homepage: www.elsevier.com/locate/ijts

Optimization of multiple heaters in a vented enclosure – A combined numerical and experimental study

T.V. Radhakrishnan [1], C. Balaji*, S.P. Venkateshan

Department of Mechanical Engineering, Indian Institute of Technology Madras, Chennai 600 036, India

ARTICLE INFO

Article history:
Received 14 April 2008
Received in revised form
29 August 2009
Accepted 28 September 2009
Available online 12 November 2009

Keywords:
Experiments
Temperature
Numerical
Optimization
Response surface
Ventilated enclosure
Heaters

ABSTRACT

This paper discusses the results of an experimental and numerical study of fluid flow and heat transfer in an enclosure where multiple heaters are arranged in a staggered fashion. Experiments were carried out for Reynolds numbers, in the range $1800 \leq Re \leq 4500$ and Grashof numbers in the range $2.5 \times 10^4 \leq Gr \leq 3 \times 10^5$. Numerical simulations were carried out for two dimensional, steady, incompressible turbulent flow and the results of the numerical study are compared with the experimental results. The temperature distribution gives an insight into the power management among the heaters, so that the "coolest" heater can be loaded most to maximize the total heat dissipation, for a prescribed temperature excess, for all the heaters. Two methods are used to achieve the target temperature for all heaters, namely (i) trial and error method and (ii) the response surface method. The latter method was adopted, to simultaneously maximize the heat input and minimize the temperature deviation from the target temperature, by employing a composite objective function. The numerically obtained optimal solution was finally verified by carrying out experiments. The method of response surface was found to be effective in optimizing the total heat transfer for a given target temperature.

1. Introduction

Printed circuit boards in electronic equipment, in general have multiple heat generating elements embedded in them. Many such printed circuit boards can be seen arranged in different slots or racks inside the equipment bay of a satellite launch vehicles and multi nodal computing systems. The cabinets are invariably cooled by air flow for low to medium heat flux levels. For carrying out a numerical analysis or experimentation, such systems can be approximated as free standing heat generating elements placed in a ventilated cavity.

A number of studies have been carried out on heat transfer from multiple heat generating elements. Both experimental and numerical investigations on natural, mixed and forced convective heat transfer from multiple heat generating elements have been reported in literature. Lai et al. [1] conducted a numerical study on mixed convection in horizontal porous layers by discrete heat sources kept at isothermal conditions. For Rayleigh numbers in the range of 10–500 and Peclet numbers in the range of 0.1–100, steady state results have been generated. The overall Nusselt numbers increased with the number of heat sources and the Rayleigh number. For Rayleigh number greater than 50, it was observed that the flow is oscillatory and unstable. Choi et al. [2] studied, numerically, heat transfer from an electronic module in an inclined cavity, for natural, mixed and forced convection regimes. The study indicated that the overall Nusselt number strongly depends on the angle of inclination.

An easy-to-use method has been developed by Funk et al. [3] to predict steady state temperatures of PCBs embedded with single or multiple heat sources. The method is based on the Green's function, wherein the heat diffusion equation is solved and is quite fast in determining the temperatures. Heindel et al. [4] studied conjugate heat transfer from multiple flush mounted heaters in a cavity. The studies have been carried out for different combinations of thermal conductivities for the wall and the fluid. For small Rayleigh numbers, the heat transfer is dominated by conduction and as the Rayleigh number increases, convective heat transfer begins to dominate. Hung et al. [5] studied, numerically, laminar flow over multiple heat sources in a horizontal channel. At the entrance to the channel, the flow is split into two, because of which the top flow impinges the heaters only partially. The bottom flow is sucked into the main flow due to pressure difference which enhances the heat transfer rate. The effect of opening at the inlet and the gap between the heat sources on the heat transfer was studied numerically.

Du et al. [6] carried out a numerical study of two dimensional steady mixed convection heat transfer in a vertical channel that had open bottom and top along with protruding discrete heaters

* Corresponding author. Tel.: +91 44 2257 4689; fax: +91 44 2257 0509.
E-mail address: balaji@iitm.ac.in (C. Balaji).
[1] Vikram Sarabhai Space Centre, Indian Space Research Organisation, Trivandrum, India.

1290-0729/$ – see front matter © 2009 Elsevier Masson SAS. All rights reserved.
doi:10.1016/j.ijthermalsci.2009.09.012

Nomenclature

A	area m^2
C_p	specific heat at constant pressure, J/kg K
C_v	specific at constant volume, J/kg K
E	total energy, J
Gr	Grashof number, $\frac{g\beta\Delta TL^3}{\nu^2}$
g	gravitational acceleration, 9.81 m/s^2
G_k	generation of turbulent kinetic energy due to mean velocity gradient, J
G_b	generation of turbulent kinetic energy due to buoyancy, J
h	heat transfer coefficient W/m^2K
I	turbulence intensity, m^2/s^2
K	turbulent kinetic energy m^2/s^2
k	thermal conductivity W/m-K
L	height of the heater, m
Nu	Nusselt number, $\frac{hL}{k}$
P	pressure Pa
Pr	Prandtl number $\frac{\mu C_p}{k}$
p	penalty parameter
Q	heat input, W
q_v	volumetric heat generation rate, W/m^3
R	universal gas-law constant, 8.314×10^3 J/kmolK
Ra	Rayleigh Number, Gr Pr
Re	Reynolds number, $\frac{uL}{\nu}$
Ri	Richardson number, $\frac{Gr}{Re^2}$
S	dimensionless length, X/W
S_k	user defined source term in RNG turbulence equation, W/m^3
S_ε	user defined source term in RNG turbulence equation, W/m^3
T	temperature, K
T_{avg}	average temperature of the heater, K
T_∞	ambient temperature, K
T_w	wall temperature, K
ΔT_{ref}	reference temperature difference, $\frac{q_v L^2}{k_s}$, K
u	horizontal component of the velocity, m/s
u_∞	inlet velocity, m/s
v	vertical component of the velocity, m/s
W	width of the chamber, mm
X	location of the heater in the horizontal direction from left wall, mm
x	horizontal distance, m
y	vertical distance, m

Greek symbols

α	thermal diffusivity, m^2/s or inverse effective Prandtl number
β	coefficient of thermal expansion, 1/K
δ_{ij}	Kronecker delta
δ	perturbation parameter
ε	emissivity of the surface or dissipation rate of turbulent kinetic energy, kg/m^2s^2
Φ	dimensionless average temperature, $\frac{T_{avg}-T_\infty}{\Delta T_{ref}}$
μ	viscosity, Ns/m^2
ν	kinematic viscosity, m^2/s
ρ	density of air, kg/m^3
σ	Stefan Boltzmann constant, $5.67x\ 10^{-8}$ W/m^2K^4
τ	shear stress, N/m^2

Subscripts

avg	average
eff	effective
∞	inlet and ambient
f	fluid
i	heater number
n	experiment number
s	solid
v	volumetric

installed on one side. Studies were carried out for $0 \leq Ra \leq 10^7$, $0 \leq Re \leq 200$ and $1 \leq A \leq 6$, where A is the aspect ratio. It was found that the entrance lengths exert a negative effect on the cooling of the components in the natural and mixed convection regimes, at low Reynolds numbers. At high Reynolds numbers, the effect of the entrance length was found to be negligible. Joseph et al. [7] also carried out experimental investigations on natural convection from embedded heat sources placed in a vertical channel. Deng et al. [8] carried out a numerical study of natural convection heat transfer in a horizontal enclosure with discrete heat sources. Heat sources of different types, orientation and size have been considered. In this study, a combined temperature scale method and a unified heat transfer characteristic analysis for convenient representation of heat transfer due to discrete heat sources were proposed.

Keyhani et al. [9] carried out an experimental study of heat transfer from discrete heater elements in a vertical cavity. In this study, unheated and heated elements of equal dimensions were mounted on one of the walls. The opposite wall was kept at a constant temperature. The heat transfer data and the flow visualization photographs indicated that stratification is the primary factor influencing the temperature of the heated sections. Sultan [10] conducted experiments to study forced convection heat transfer from multiple protruding heat sources in a horizontal channel of small aspect ratio with passive cooling. Perforated holes were arranged at the base of channel in a staggered manner in two rows between the heat sources. Due to an increase of the temperature between the heaters, the outside air is drawn naturally through the perforated holes. The effect of the size of holes on the heat transfer for a range of Reynolds numbers was studied. It was found that the heat transfer coefficient was enhanced for all values of the hole/open area ratio. However, holes with $\beta = 0.0409$ gave the best thermal performance for $376 < Re < 6170$, where β is the ratio of total hole area to one side area of the heater.

Rodgers et al. [11] carried out a numerical study of forced convection from printed circuit boards with heat generating elements and verified its accuracy based on experiments. The heat sources used were SO16, TSOP 48 and PQFP 208 [12] packages. The objective of the study was to create bench mark test data for numerical modeling. Baskaya et al. [13] investigated, experimentally, heat transfer from an array of heat sources in a rectangular channel, in the mixed convection regime. The configuration was typically an electronic package. It was observed that when the Reynolds number decreased and/or Grashof number increased, an enhancement in heat transfer was obtained through buoyancy driven secondary flow. The study gave guidelines for the placement of electronic packages subjected to flow in a rectangular channel.

The above discussion focused on numerical and experimental studies on heat transfer and flow characteristics for multiple heat generating elements. Optimization methods and studies applicable to multiple heat generating elements, most of which are numerical, are discussed next.

Perez et al. [14] used a quadratic response surface approximation for engineering design problems. A methodology to reduce the size

of the database required for building a response surface was presented. Wang et al. [15] dealt with an adaptive surface optimization method for thermal optimization related to an aircraft engine cooling system, in considerable detail. The overall aim of the study was to improve the thermal effectiveness of an aircraft design strategy. Rodriguez et al. [16] presented a response surface based optimization scheme using a Cartesian CFD method for the aerodynamic design of aircraft. For a supersonic aircraft, the response surface based optimization scheme coupled with the Euler solver worked well. The method was found to be effective for the optimization of all the components but was limited by the number of variables.

Cheng et al. [17] carried out an interesting study for packages in order to enhance the cooling of multiple heater elements. The study was concerned with the determination of the optimal shape for a package containing multiple heating elements. The optimization tool was developed based on the inverse heat transfer (IHT) approach, incorporating a direct problem solver, a numerical grid generator, a direct-differentiation sensitivity analyzer, and the conjugate gradient method. The shape design that leads to a specified outer surface temperature distribution was predicted by the approach. da Silva et al. [18] investigated the optimal placement of heat sources on a vertical wall at discrete locations. The investigation pointed out that there can be optimal locations with the objective of global performance and minimization of thermal resistance between the substrate and the fluid. It was observed that the maximized global conductance was independent of Ra for $Ra < 10^4$. However, it proportionately increased for $Ra > 10^4$.

To reduce the computational effort during the optimization process, Lee et al. [19] used a refined response surface method to design nose fairings of a space launcher. The total drag was selected as the objective function, and the surface heat transfer, the fitness ratio and the internal volume of the nose fairing were considered as design constraints. Park et al. [20] used a progressive quadratic response surface model for the optimal design of heat exchangers. The objective here was to minimize the pressure loss in the system under the required temperature rise. The solution compared well with solutions obtained through other optimization techniques. The shape optimization of a dimpled channel to enhance turbulent heat transfer was reported by Kim et al. [21]. Kim et al. [22] used the response surface method for optimizing the design of a rectangular channel with inclined ribs to enhance turbulent heat transfer. Optimum shapes of the channel have been obtained in a range of the weighting factor corresponding to heat transfer and friction loss related terms. Cheng et al. [23] evolved an effective method to deal with the optimization problem in multiple chip modules. To reduce the computational time, they effectively used the response surface and curve fitting techniques.

In this paper, numerical simulations and experimental investigation of convective heat transfer from heater elements arranged in a staggered manner in a ventilated cavity is discussed. The study aims at the evaluation of the operating temperature of each heater. The temperature distribution gives an insight into the power management among the heaters, so that the coolest heater can be loaded more, to maximize the total heat dissipation, for a prescribed temperature excess for all the heaters. From the review of literature presented above, it is seen that comprehensive investigations on this subject are not reported in literature, though the problem under consideration is of great practical interest.

2. Experimental arrangement

Fig. 1 shows a schematic of the experimental set up used for the study. The set up consists of a chamber, the inside of which is well insulated with 10 mm thick wooden panels on all sides. Hence, the walls can be considered as insulated. The joints were further insulated with Teflon tapes to avoid any heat leak to outside. Air

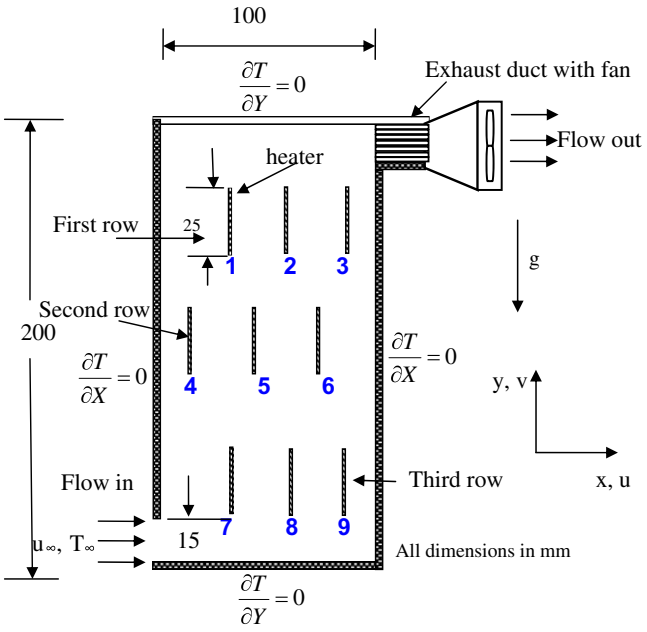

Fig. 1. Schematic of the multiple heater arrangement for experiments and boundary conditions used in numerical simulations.

enters the cavity through a slit (inlet port) provided at the bottom and leaves through another slit (outlet port) at the top of the right wall as shown in Fig. 1. The ports are in a direction perpendicular to the plane of the paper. The inlet and outlet ports, are rectangular slits, of dimensions 15 × 150 mm. A rectangular duct with a conical section is provided at the outlet port fitted with an axial flow fan to create the necessary air flow within the chamber. The speed of the fan can be regulated to carry out experiments at different Reynolds numbers. Nine heaters of size 25 mm × 150 mm with 3 mm thickness are fastened on wooden walls at the two ends of the chamber through grooves. Heaters are thin foil type, and are sandwiched between aluminum sheets of 1.25 mm thickness. The overall thickness of the heater after the assembly is 3 mm. The heater surfaces are highly polished to minimize heat loss by radiation. Each heater is connected to an individual DC power supply. This facilitates control of power supply to each heater based on the requirements. A thermo-anemometer is used to measure the air velocity at the inlet. Experiments were carried out for different Reynolds numbers and varied power inputs to heaters.

3. Numerical simulations

This section gives the details of the numerical modeling and the solution procedure.

3.1. Problem definition and boundary conditions

The problem and boundary conditions for the numerical simulation are depicted in the schematic given in Fig. 1. The air enters from the bottom part of the left side wall and leaves the chamber through a port provided at the top of the right side wall of the chamber.

Assumptions

(1) All external boundaries are insulated.
(2) Thermophysical properties are constant.
(3) The velocity at the inlet is uniform.
(4) The flow is two dimensional and steady.
(5) Heat generation is uniform within any heater.

(6) Boussinesq approximation is valid for modeling the density variation.
(7) Heaters are highly polished and so heat loss due to radiation is negligible.

3.2. Governing equations for modeling the heat transfer

The governing equations for steady, two dimensional, turbulent, incompressible flow with heat transfer is given by the well known Reynolds averaged Navier–Stokes equation and the equation of energy. For a Cartesian co-ordinate system these are,

Continuity Equation:

$$\frac{\partial u}{\partial x}+\frac{\partial v}{\partial y}=0 \tag{1}$$

Momentum Equations:

$$\rho\left[u\frac{\partial u}{\partial x}+v\frac{\partial u}{\partial y}\right] = -\frac{\partial P}{\partial x}+\frac{\partial}{\partial x}\left[2(\mu+\mu_t)\frac{\partial u}{\partial x}\right] +\frac{\partial}{\partial y}\left[(\mu+\mu_t)\left(\frac{\partial u}{\partial y}+\frac{\partial v}{\partial x}\right)\right] \tag{2}$$

$$\rho\left[u\frac{\partial v}{\partial x}+v\frac{\partial v}{\partial y}\right] = -\frac{\partial P}{\partial y}+\frac{\partial}{\partial x}\left[(\mu+\mu_t)\left(\frac{\partial v}{\partial x}+\frac{\partial u}{\partial y}\right)\right] +\frac{\partial}{\partial y}\left[2(\mu+\mu_t)\frac{\partial v}{\partial y}\right]-\rho g \tag{3}$$

The conservation of momentum in the horizontal (x) and vertical (y) directions in an inertial reference frame is represented by eqns. (2) and (3) respectively. In eqns. (2) and (3) p is the static pressure and the terms in the brackets on the right hand side represent the viscous shear stresses. The term, ρg in equation (3) represents the buoyancy force.

Energy Equation:

$$\rho C_p\left[u\frac{\partial T}{\partial x}+v\frac{\partial T}{\partial y}\right] = \frac{\partial}{\partial x}\left[(k+k_t)\frac{\partial T}{\partial x}\right]+\frac{\partial}{\partial y}\left[(k+k_t)\frac{\partial T}{\partial y}\right] \tag{4}$$

Where the turbulent thermal conductivity, $k_t = C_p\ \mu_t/Pr_t$. The energy equation applicable for incompressible flow is given in eqn. (4). The terms on the left hand side represent the energy transported due to convection and those on the right hand side represent the energy transported due to diffusion that also includes transport of energy by turbulence.

3.2.1. Turbulent flows

The geometry and the flow regime call for modeling the turbulence in the flow. Turbulent flows are characterized by fluctuating velocity fields. These result in the mixing of transported quantities such as momentum and energy. The fluctuations of these quantities are normally of small scale and high frequency. Hence, it is computationally more expensive to simulate such flows. These equations are converted into time averaged or ensemble averaged instantaneous (exact) governing equations. These equations are further manipulated to remove small scales thereby resulting in modified equations that are computationally less expensive. The additional terms in the above equations due to turbulence (μ_t, Pr_t) are to be modeled separately.

3.2.1.1. RNG k-ε model. Henkes et al. (1991) pointed out that for large Rayleigh numbers ($>10^9$), the boundary layer at the heated wall becomes thin, leading to large gradients near the wall. Consequently, very fine meshes are required in this region to capture the gradients. Furthermore, their simulations showed that for turbulence modeling, the standard k-ε model over predicts the heat transfer, whereas the low Reynolds number k-ε models of Chien (1980), and Jones and Launder (1972) are reasonably close to experiments. For the problem under consideration, preliminary calculations with the standard k-ε model resulted in difficulties with convergence. However, the RNG k-ε model gave convergent results that are in reasonably good agreement with measured temperatures.

Hence, for further calculations the k-ε (RNG) model is adopted for the turbulence closure. The RNG based k-ε model is derived from the instantaneous Navier–Stokes equations, using a mathematical technique called "renormalization group" or RNG method. The analytical derivation leads to a model whose constants are different from those used in the standard k-ε model.

$$\frac{\partial}{\partial x}(\rho k u)+\frac{\partial}{\partial y}(\rho k v)=\frac{\partial}{\partial x}\left[\alpha_k\mu_{\text{eff}}\frac{\partial k}{\partial x}\right]+\frac{\partial}{\partial y}\left[\alpha_k\mu_{\text{eff}}\frac{\partial k}{\partial y}\right]G_k+G_b-\rho\varepsilon \tag{5}$$

$$\frac{\partial}{\partial x}(\rho\varepsilon u)+\frac{\partial}{\partial y}(\rho\varepsilon v) = \frac{\partial}{\partial x}\left[\alpha_\varepsilon\mu_{\text{eff}}\frac{\partial \varepsilon}{\partial x}\right]+\frac{\partial}{\partial y}\left[\alpha_\varepsilon\mu_{\text{eff}}\frac{\partial \varepsilon}{\partial y}\right] +C_{1\varepsilon}\frac{\varepsilon}{k}(G_k+C_{3\varepsilon}G_b)-C_{2\varepsilon}\rho\frac{\varepsilon^2}{k}-R_\varepsilon \tag{6}$$

the quantities α_k and α_ε are the inverse effective Prandtl numbers for k and ε respectively.

The effective thermal diffusivity, k_{eff} in the RNG turbulence model is,

$$k_{\text{eff}} = \alpha c_p\mu_{\text{eff}} \tag{7}$$

The effective viscosity, μ_{eff}, in equation (7) can be determined through the scale elimination procedure in the RNG theory. This results in the following differential equation for turbulent viscosity.

$$\mathrm{d}\left(\frac{\rho k^2}{\sqrt{\varepsilon\mu}}\right) = 1.72\ \frac{\nu}{\sqrt{\hat{\nu}^3-1+C_\nu}}\,\mathrm{d}\hat{\nu} \tag{8}$$

$$\hat{\nu} = \frac{\mu_{\text{eff}}}{\mu} \tag{9}$$

$$C_\nu \approx 100 \tag{10}$$

The equation for turbulent viscosity is integrated to obtain an accurate description of how the effective turbulent transport varies with effective Reynolds number and the near-wall flow.

In the high Reynolds number limit

$$\mu_t = \rho C_\mu\frac{k^2}{\varepsilon} \tag{11}$$

The constant, C_μ is 0.0845 in equation (11) is derived using RNG theory. It is very close to 0.09 used in the standard k-ε model. The RNG k-ε model requires the turbulent intensity, I and the length scale, l to be specified. The turbulence intensity, I is the ratio of root-mean-square of the velocity fluctuations, u', to the mean flow velocity, u_{avg}. A turbulence intensity less than 1% means low intensity and a value greater than 10% represents high intensity. The turbulence intensity can be specified as a function of Re and is given by,

$$I = 0.7\,\mathrm{Re}^{-0.8} \tag{12}$$

The turbulence length scale, l, is a physical quantity related to the size of the large eddies that contain the energy in the turbulent flows. l is related to the length scale at the inlet and is given by,

$$l = 0.07\,L \tag{13}$$

where L is the characteristic length of the inlet.

3.2.1.2. Near-wall treatment for wall-bounded turbulent flows. Turbulent flows are affected by the presence of wall. The mean velocity is affected by the condition of no-slip at the wall. Very close to the wall there is viscous damping which reduces the tangential velocity fluctuations. At the outer part of the near-wall region, turbulence is rapidly augmented by the production of turbulent kinetic energy due to large gradients in the mean velocity. The solution of the flow with turbulence is significantly affected by near-wall modeling. Hence, an accurate representation of the flow near the wall region determines the accuracy of the prediction of wall-bounded flows. The near-wall flow can be treated in two ways (1) by using wall functions and (2) by wall treatment. In the first method, the viscous sub-layer and the buffer layer – the viscosity affected region, close to the wall are not resolved. These regions are modeled using semi empirical formulae called "wall functions" to bridge them with the fully turbulent outer flow. Hence, the use of wall functions eliminates the requirement of any modifications in the turbulence model. In the second method, the viscosity affected region is fully resolved from turbulent region up to the wall. For low velocity flows, the enhanced wall treatment is ideal. The meshing near the wall should be fine enough so that at the wall the dimensionless wall co-ordinate $y^+ < 5$.

3.3. Solution procedure

Computations have been carried out using FLUENT 6.2, a commercially available software. Segregated, implicit, 2-D, steady incompressible flow solver has been employed for the numerical study. The velocity and temperature gradients are cell based. The SIMPLE algorithm with second order up winding for momentum and energy is used. A typical grid pattern employed in the study is given in Fig. 2. The convergence criterion is 10^{-3} on all primary variables, k and ε. It is 0.1% on both mass and energy balance. The mesh size has been selected such that the wall y^+ values are found to be less than 5 for all the cases.

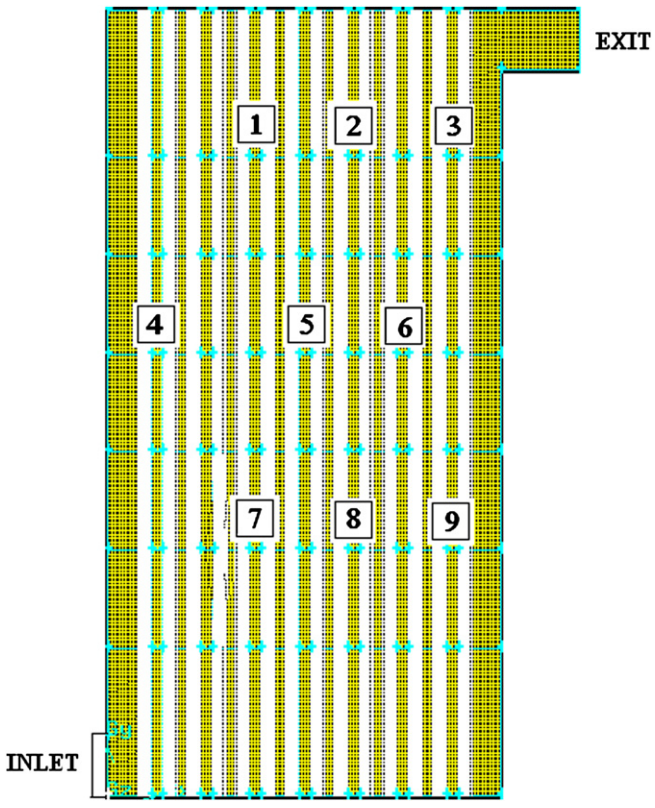

Fig. 2. Grid structure used for simulations (1–9 represent heaters).

4. Optimization studies

As mentioned in the introduction, electronic equipment operate on a safe operating temperature range. For example, the equipment bay in a satellite launch vehicle has a safe operating temperature of 10–60 °C. Hence, heaters have to be arranged such that no heater temperature shall exceed this limiting temperature of 60 °C. Furthermore, the heater elements have to be located judiciously, such that the elements which require large heat dissipation are cooled effectively. Such heaters have to be placed within the flow so that a maximization of the power input to the heaters is also possible.

4.1. Trial and error method

In the trial and error method, the optimal heat distribution of heaters is achieved through a judicious perturbation of the power distribution based on plots of temperatures vs. volumetric heat generation rates. It is possible from these plots to arrive at the heat generation rate of each individual heater so as to achieve a "target" temperature, such as 333 or 353 K. Initially, for an arbitrary distribution of constant heat input, the temperature of each heater is determined using numerical simulations. From the resultant temperature distribution, one can decide in which direction the heat input has to be varied in order to approach target temperature for all the heaters. With a systematic adjustment of heat input and by studying the temperature distribution carefully, via a trial and error method the target temperatures are achieved.

The method adopted for the trial and error is summarized below,

(a) For a constant heat input to all heaters, generate temperature distribution using simulations.
(b) Estimate the difference between the simulated and target temperature for each heater.
(c) Increase or decrease the heat input to each heater according to the deviation.
(d) Repeat the above steps until the target temperature is achieved within an error band.

The main disadvantage of the trial and error method is that for each temperature, we have to conduct a number of numerical experiments. To overcome this problem, a better method, based on response surfaces is adopted.

4.2. Method of response surface

This method finds application in chemical processes, agriculture, business and so on wherein the objective function, a function of several independent variables is extremized. A response surface is primarily a simplified form of a surface fit involving multiple parameters. Hence, it can be assumed as a multidimensional surface fit. The functions forming the surface fit are normally nonlinear (Khuri et al. [24]).

An important variant of the response surface method is the adaptive response surface method for optimization, which is a global optimization technique. The main feature of this method is that, it fits a quadratic approximation for the function that has to be optimized. The method is an effective tool when the number of design variables is low, normally between 2 and 10. The efficiency of the method depends on how the surface fit represents the actual function that it has to mimic.

The response surface methodology involves the following steps.

(a) Carrying out designed numerical or actual experiments to yield adequate and reliable measurements of interest.
(b) Determining a mathematical model involving measured parameters which has to be tested for its verification.
(c) Determination of optimal setting of values which satisfies the maximum or minimum value of the response.

In any system in which the variable quantities change as in experiments, the results also change. The effect of each parameter on the measurements can be assessed through regression analysis. Regression analysis helps us in formulating a relation between dependent and independent parameters, though empirically.

We can have a function, η of type,

$$\eta = P(X_1, X_2, \ldots\ldots X_k) \tag{14}$$

Where, X_1, X_2 … X_k represent the independent variables. In the present case X_1, X_2… X_k are powers (heat inputs) and η is the temperature of a particular heater. We have to develop an equation for the temperature of each heater in terms of heat inputs to all the heaters. We know that the temperature of each heater primarily depends on its own heat input and to a lesser extant on the temperature of other heaters. Hence, a cubical variation is considered for the heater in question and quadratic variation is considered for the near by heaters and a linear variation is assumed for all other heaters away from the heater.

Let Q_{1n}, Q_{2n}, Q_{3n}, Q_{4n}, Q_{5n}, Q_{6n}, Q_{7n}, Q_{8n} and Q_{9n} be heat inputs to heaters 1–9 and T_{1n}–T_{9n} be temperatures of the respective heaters in the nth experiment. We can have an equation for T_{1n} as,

$$\begin{aligned} T_{1n} = {} & a_0 + a_1 Q_{1n}^3 + a_2 Q_{1n}^2 + a_3 Q_{1n} + a_4 Q_{2n}^2 + a_5 Q_{2n} \\ & + a_6 Q_{3n}^2 + a_7 Q_{3n} + a_8 Q_{4n} + a_9 Q_{5n} + a_{10} Q_{6n} \\ & + a_{11} Q_{7n} + a_{12} Q_{8n} + a_{13} Q_{9n} \end{aligned} \tag{15}$$

The coefficients, a_o to a_{13} are unique to heater 1. These coefficients carry a different value for heater 2, heater 3 and so on. For the sake of convenience and clarity, the coefficients for heater 2 are denoted by b_o to b_{14}. Hence the temperature T_{2n} for the heater 2 can be written as,

$$\begin{aligned} T_{2n} = {} & b_0 + b_1 Q_{2n}^3 + b_2 Q_{2n}^2 + b_3 Q_{2n} + b_4 Q_{1n}^2 + b_5 Q_{1n} \\ & + b_6 Q_{3n}^2 + b_7 Q_{3n} + b_8 Q_{4n} + b_9 Q_{5n} + b_{10} Q_{6n} \\ & + b_{11} Q_{7n} + b_{12} Q_{8n} + b_{13} Q_{9n} \end{aligned} \tag{16}$$

Similarly, for all heaters such equations can be formed. The above coefficients have to be evaluated through regression analysis. Matrix inversion technique has been adopted for this purpose. If there are 'n' number of experiments in which the heat input and temperature distributions are available, a matrix equation can be formed as,

$$[A][C] = [T] \tag{17}$$

where $[A]$ is the dependent variable matrix, $[C]$ the coefficient matrix and $[T]$ is the temperature matrix of the heater for all 'n' experiments.

For example, in the case of heater 1 the dependent variable matrix $[A]$ depicted in eqn. (17) can be represented as,

$$A1 = \begin{bmatrix} 1 & Q_{11}^3 & Q_{11}^2 & Q_{11}Q_{21}^2 & Q_{21} & Q_{91} \\ 1 & Q_{12}^3 & Q_{12}^2 & Q_{12}Q_{22}^2 & Q_{22} & Q_{92} \\ 1 & Q_{1n}^3 & Q_{1n}^2 & Q_{1n}Q_{2n}^2 & Q_{2n} & Q_{9n} \end{bmatrix}$$

Note that the first row is formed by distribution of heat inputs for 9 heaters in the first experiment and similarly the last row is formed using data available for nth experiment. In the first row Q_{11} means heat input of heater 1 in the experiment 1. Similarly Q_{13} represents heat input of heater 1 in the third experiment and so on. The second subscript represents the experiment number.

The coefficient matrix, $[C]$ and temperature matrix, $[T]$ in eqn. (17), for heater 1 is respectively represented as,

$$C1 = \begin{bmatrix} a_0 \\ a_1 \\ \\ a_{13} \end{bmatrix}, \quad T1 = \begin{bmatrix} T_{11} \\ T_{12} \\ \\ T1n \end{bmatrix}$$

As mentioned earlier, the coefficients within the matrix are unique to heater 1.

It is to be noted that the temperatures shown in the matrix T_1 are for heater 1 in all the 'n' experiments starting from 1. Here we have

$$[C1] = [A1]^{-1}[T1] \tag{18}$$

The above equation should predict the temperature for the heater 1 for any heat distribution within the experimental range. Similarly, equations are constructed for the other 8 heaters. The setting up of equations is the first phase of the method. In the second phase, the equations already derived are used to predict the temperatures for random heat inputs. Using the method of elimination, the best suited combination is selected. The process is further refined by perturbing the selected heat distribution. The steps are repeated till convergence of the desired objective function (which will be discussed subsequently) is satisfied. MATLAB software version 6.7 was used for this purpose. The method adopts two phases for present analysis as given below:

Phase 1
a. Using CFD simulations, predict temperature data for each heater using random heat distributions to all heaters.
b. Establish a correlation for temperature of each heater, as a function of heat input to all heaters. In the present case, there will be 9 correlations for the 9 heaters.

Phase 2
The goal of this phase is to maximize the objective function,

$$Y = \sum_{i=1}^{i=9} \left[Q_i - \lambda (T_i - T_{\text{target}})^2 \right] \tag{19}$$

Where, λ is the penalty parameter. The objective function Y is a composite objective function involving the maximization of power input and minimization of error in target temperatures. As the deviations in the heater temperatures from their target values decrease, the second term tends to zero. Hence, the value of λ should be positive, to maximize the total heat input. The optimization procedure is as follows:

1. Choose an average heat distribution for all heaters as an initial guess.
2. Randomly generate a number of combinations by perturbing the initial guess values, keeping the maximum and minimum limit for each heater (subject to the rating of the heater).
3. Generate a temperature distribution for each set using the correlations in step b of Phase 1.
4. When the best Q's are obtained with the largest possible Y, stop the iterative process.

If λ is very large, say 10^6, and there exists a large error in the temperature, the second term will be large and the function will have a negative value and hence such a solution is not acceptable. As already mentioned, λ will be positive and a sensitivity study

is required for finalizing its value while determining the optimal solution. The procedure followed for achieving the target temperatures using the adaptive method is represented as a block diagram in Fig. 3, depicting all the steps described above.

The correlation derived in phase 1 is used in phase 2 for computation of the temperatures of the individual heaters for the random distribution of heat inputs generated by the algorithm.

5. Results and discussion

5.1. Experimental uncertainty

During the experiments, individual heater temperatures, ambient temperatures and inlet velocities are measured. The Reynolds number is computed based on the inlet velocity and heater height. The Grashof numbers for the heaters are computed based on the temperature difference between average temperature of the heater measured in the experiment and the inlet temperature. Calibrated thermocouples were used for measurements and there exists a deviation of ±0.125% of the actual reading. The air velocity is measured with an uncertainty of ±1% as specified by the manufacturer. An estimate of the error in the experimental data has been carried out, based on standard techniques due to Kline and Mcclintock [25]. The error in the Nusselt number is found to be ±6–7% and for the Reynolds number, the error is ±7–9%.

5.2. Experimental results

Experiments are carried out for Reynolds numbers, in the range $1800 \leq Re \leq 4500$ and Grashof numbers in the range $2.5 \times 10^4 \leq Gr \leq 3 \times 10^5$. Figs. 4–6 show the variation of the Nusselt number of the heaters with Grashof number, at various Reynolds number (Re = 1800, 3600, 4500). It can be seen that the variation of Nusselt number for heater 3 with respect to Grashof number is not uniform. For low Reynolds number (Fig. 4) the Nusselt number shows an increasing trend with Grashof number due to the effect of buoyancy which helps in augmenting the flow.

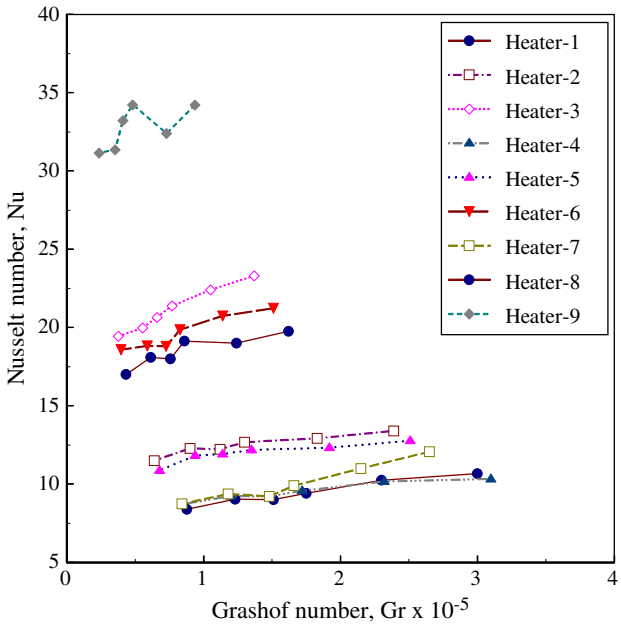

Fig. 4. Variation of Nusselt number with Grashof number for all the heaters, Re = 1800.

As the Reynolds number increases the trend reverses (Fig. 6) since the flow becomes forced convection dominant. In all the cases, heater 3 witnesses the highest heat transfer rate, if we consider the top row of heaters. The temperature of heater 2 is found to be between those of heaters 1 and 3. This is due to the influence of heater 3, as some of the fluid is deflected towards heater 2 and hence the heat transfer rate is marginally more compared to heater 1. For heaters 1 and 2,

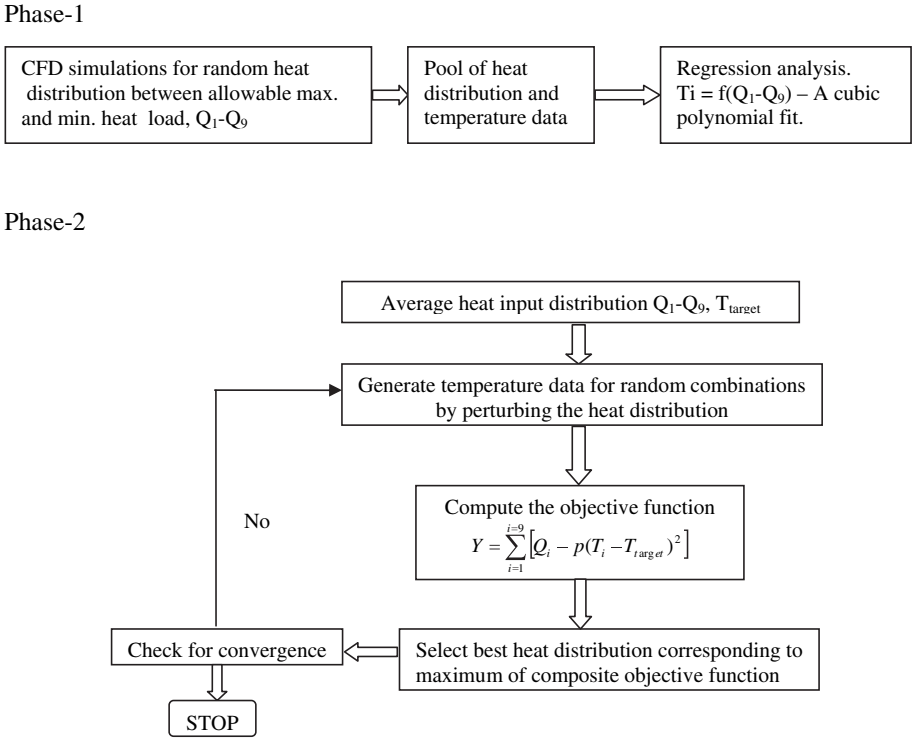

Fig. 3. Block diagram for the optimization algorithm.

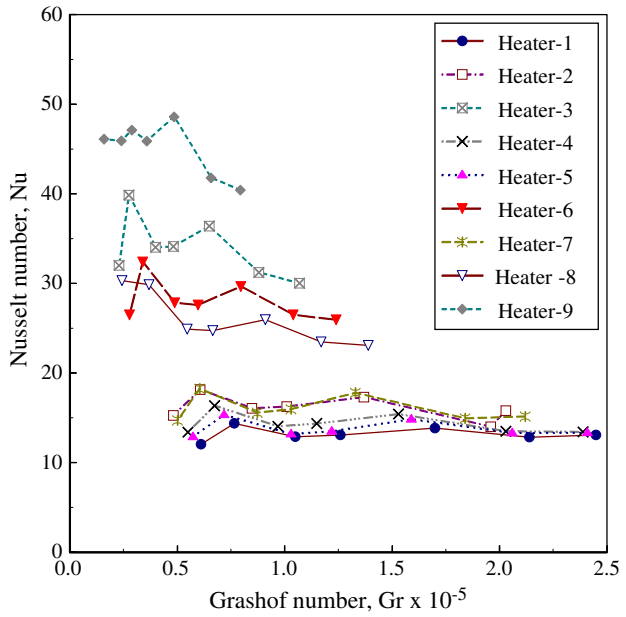

Fig. 5. Variation of Nusselt number with Grashof number for all the heaters, Re = 3600.

the variation of Nusselt number with Grashof number seems to be marginal. This is due to the fact that these heaters are not much affected by flow. However, there is a small increase in the Nusselt number for Re = 1800 with Grashof number, which is a consequence of buoyancy aiding heat transfer, as already indicated.

Figs. 4–6 also show the variation of Nusselt number with Grashof number, for heaters placed in the second row (heaters 4, 5 and 6) for Reynolds numbers 1800, 3600 and 4500 respectively. Observations similar to those for the first row of heaters may be made for these also. As expected, with an increase in Grashof number, the Nusselt number decreases, even though it is not to a significant extent. At low Reynolds numbers, the effect of buoyancy is clearly seen, as the Nusselt number increases with increasing Grashof numbers. As in the previous case, heater 6 located near right wall experiences the highest heat transfer rate.

Similarly, Figs. 4–6 show the variation of Nusselt number with Grashof number for heaters 7, 8 and 9 for Re = 1800, 3600 and 4500 respectively placed in the third row. It is observed that for Re = 1800, the effect of buoyancy is seen for all the heaters. As the Grashof number increases, especially at Re = 4500, the Nusselt number for heater 9 decreases rapidly. However, the decrease in Nusselt number for heaters 7 and 8 is very small. Again, heater 9 witnesses the highest heat transfer rate. It can be seen that with an increase in the Reynolds number, the heat transfer rate also increases for all the heaters. Heater 9 in the bottom row at the extreme right near the wall is cooled more

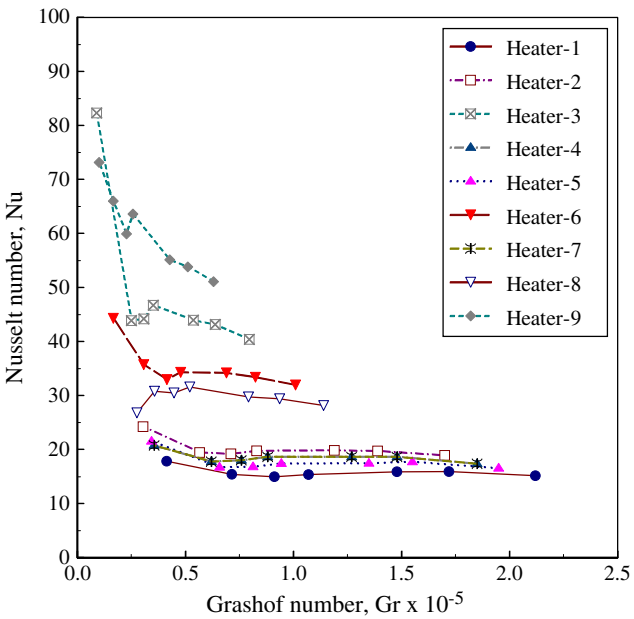

Fig. 6. Variation of Nusselt number with Grashof number for all the heaters, Re = 4500.

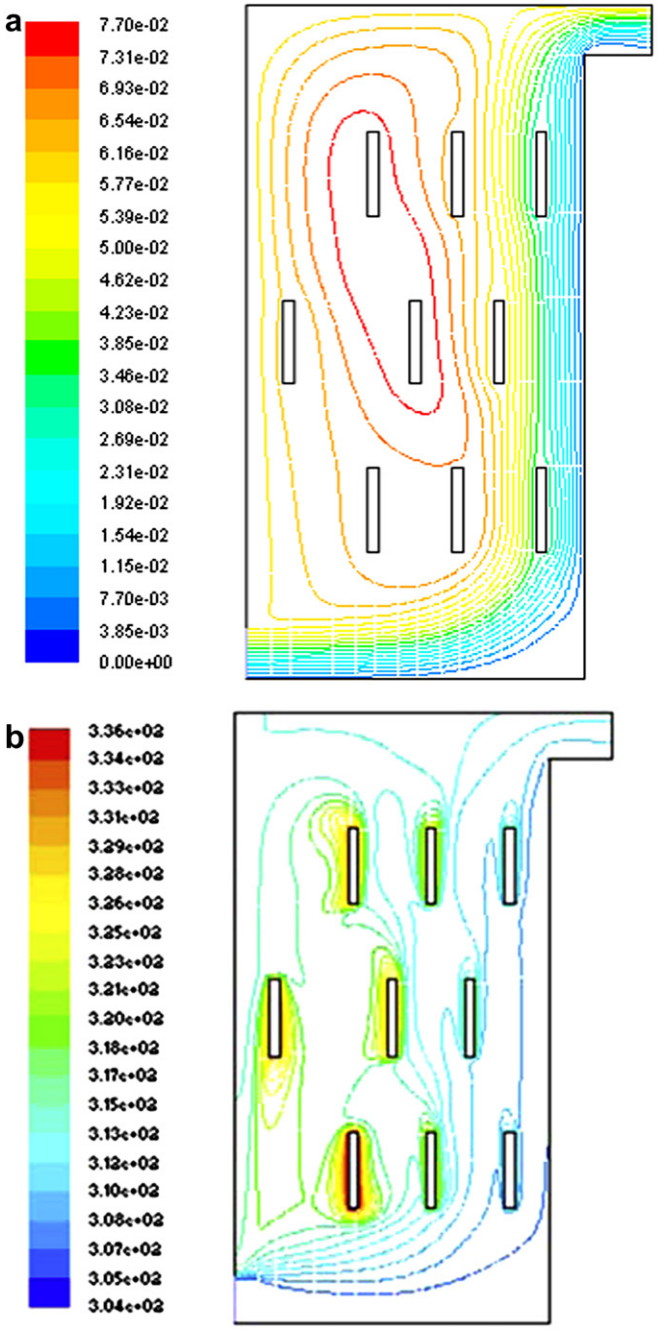

Fig. 7. (a) Streamlines for u_∞ = 3 m/s and $q_v = 1.5 \times 10^5$ W/m^3. (b) Isotherms for u_∞ = 3 m/s and $q_v = 1.5 \times 10^5$ W/m^3.

effectively compared to others. Heater 6, which is away from the wall, shows a lower heat transfer rate compared to heaters 3 and 9.

The heat transfer rate from heater 8 is more compared to those from heaters from 2 to 5. It is seen that the difference in heat transfer rates between heaters 4 and 5 reduces when the Reynolds number increases. It is interesting to note that, with an increase in the Grashof number, the heat transfer from heaters 3, 6 and 9 shows a decreasing trend. However, other heaters show nearly constant heat transfer rate as they are barely affected by the flow. For heaters within the flow at low Grashof numbers, the heater temperature rise is very low, leading to high Nusselt numbers, whereas for heaters in other locations, even at low Grashof numbers there is appreciable rise in temperature, leading to low Nusselt numbers. As the Grashof number increases, the temperature increases and so the heat transfer coefficient and the Nusselt numbers decrease. However, for the low Nusselt number cases (heaters located in the stagnant area or away from the flow path) heaters are already at elevated temperatures and hence with an increase in Grashof number, the temperature increase is not appreciable.

It is clear from the above figures that at high Reynolds numbers, trend lines showing Nusselt number variation for heaters 1, 2, 4, 5 and 7 are clustered together. When the Reynolds number is low (Re = 1800), trend lines for the middle heaters 2 and 5 separate out and form a separate group as seen in Fig. 4. In all the cases, however, heater 9 shows the maximum heat transfer rate.

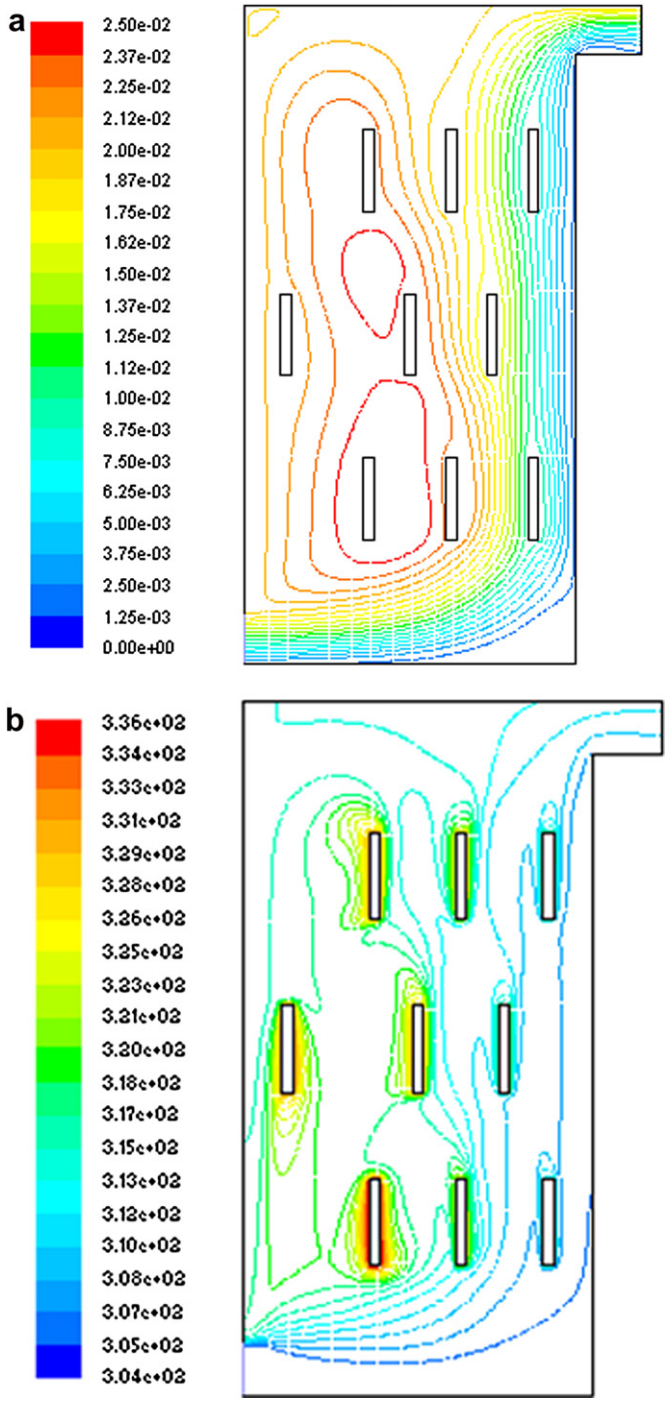

Fig. 8. (a) Streamlines for $u_\infty = 1$ m/s and $q_v = 1.5 \times 10^5$ W/m^3. (b) Isotherms for $u_\infty = 1$ m/s and $q_v = 1.5 \times 10^5$ W/m^3.

5.3. Flow and heat transfer characteristics (numerical results)

Figs. 7a,b and 8a,b show the streamlines and isotherms for inlet velocities of 3 m/s and 1 m/s respectively. For a velocity of 3 m/s, the fluid flow is concentrated towards the right wall, whereas at a low velocity of 1 m/s the fluid starts spreading immediately after entering the cavity. It is seen that the heater near the right hand wall actually deflects the flow towards the inside and hence helps in heat transfer from the outer heaters.

A comparison of temperatures obtained from numerical simulations and the measurements for, q_v of 1.5×10^5 W/m^3 is given in Table 1. The deviation between experimental and numerical temperature values is also given in the Table. It can be seen that for most of the heaters the agreement between the two is good.

Fig. 9 shows a comparison of the numerical and experimental results for cases runs with the same Reynolds number and heat input to all heaters. In this figure, the results of four experimental runs were compared with the corresponding numerical simulations. The Reynolds number for the experiments are 1500 ($u_\infty = 1$ m/s) and 4500 ($u_\infty = 3$ m/s). The volumetric heat generation rates are 1.5×10^5 and 2.2×10^5 W/m^3. From the figure, it is clear that there is a slight bias, as the predicted temperature is somewhat higher than the experimental results. This is due to uncertainties in the modeling compared to experimentation. However, the results indicate the trend decisively and deviations beyond 2% are none. The percentage increase in the Nusselt number from Re = 1500 to 4500 for different heaters is given in Table 2. The Nusselt numbers for heaters 3, 6 and 9 show that these heaters are cooled to a substantially better extent compared to heaters 2, 5 and 8. The heat transfer rate of heaters 1, 4 and 7 are low compared to the rest of the heaters.

It is interesting to note that the percentage increase in the Nusselt number for the middle heaters is low compared to the heaters on either side particularly for high values of Re. This may be due to

Table 1
Comparison of measured and numerically simulated temperatures for the multiple heater configuration for $q_v = 1.5 \times 10^5$ W/m^3 for all heaters.

Heater	Re = 1500			Re = 3500			Re = 4500		
	Temp. (exptl)	Temp. (num)	% diff	Temp. (expt)	Temp. (num)	% diff	Temp. (expt)	Temp. (num)	% diff
1	332.1	329.7	0.70	323.1	322.5	0.19	316.0	320.7	1.48
2	324.6	323.2	0.46	319.1	317.7	0.44	312.5	316.3	1.21
3	316. 5	316.0	0.14	311.2	310.6	0.19	305.8	309.4	1.17
4	331.1	331.7	0.20	321.2	320.3	0.28	314.1	317.82	1.18
5	325.8	329.3	1.07	321.9	322.6	0.21	312.4	320.3	2.53
6	317.0	317.7	0.22	312.7	313.0	0.09	308.2	311.8	1.16
7	331.0	335.9	1.50	319.7	326.0	1.98	312.2	323.5	3.63
8	318.2	322.3	1.30	311.6	319.5	2.53	311.6	318.2	2.11
9	312.0	313.5	0.48	309.0	309.0	0	306.2	308.2	0.66

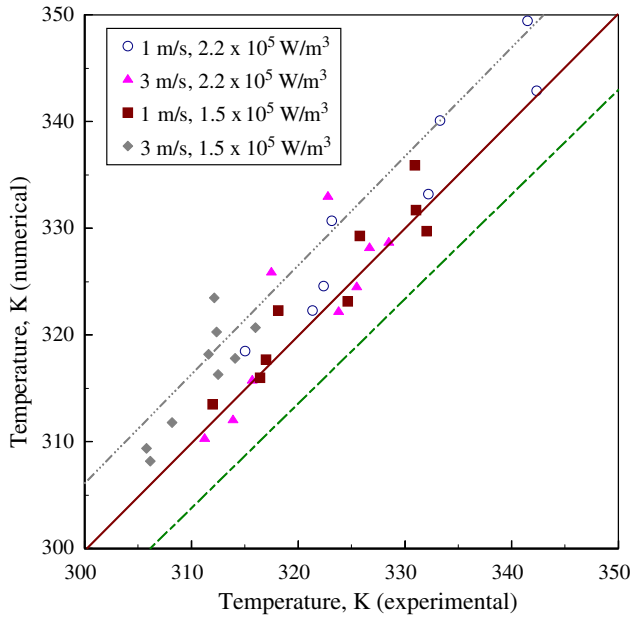

Fig. 9. Parity plot between measured and computed temperatures.

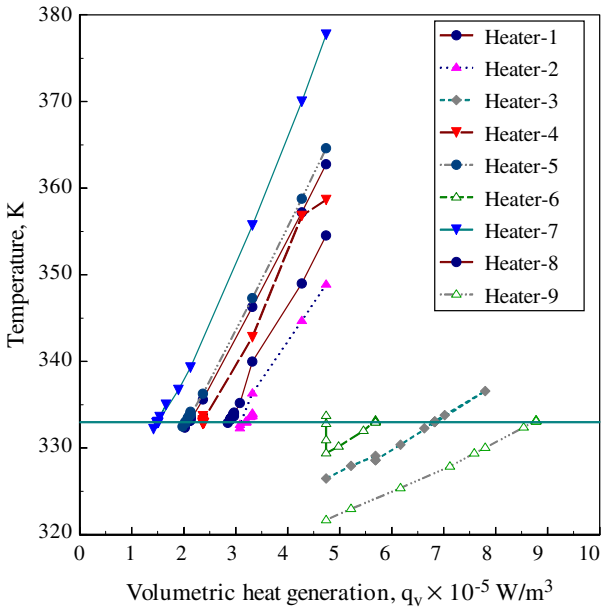

Fig. 10. Temperature plot showing approach to target temperature (333 K).

increased circulations at higher velocities and the end heaters benefit from this circulation.

5.4. Results and discussion (optimization studies)

5.4.1. Trial and error method

Section 4.1 detailed the procedure followed for achieving a target temperature using the trial and error method. Fig. 10 shows the response of the different heaters to varying volumetric heat generation, when the target temperature is 333 K. Initially, when a power input of 4.75×10^5 W/m^3 was given to all the heaters, it resulted in higher temperatures for heaters 1, 2, 4, 5, 7 and 8, whereas heaters 3, 6 and 9 showed lower temperatures. A study of this temperature distribution for a given power input suggests the direction in which we have to control the power inputs to achieve a given target temperature. It is clear from the figure that heater 9 can be loaded to a larger extent compared to other heaters.

5.4.2. Response surface method

A detailed description on the response surface adopted has been given in Section 4.2. Fig. 11 shows the convergence of temperatures to a target temperature of 333 K after 20 iterations. It should be noted that after the first iteration, the maximum deviation from the target temperature is 22.5 °C and subsequently as the iterations proceed, convergence to the target temperatures within an error band of ±2 °C is achieved.

Furthermore, the final solution also depends on number of data generated (population) in each iteration. The population of heat input is generated in the following way. Let the heater average power distribution, Q_{avg} be 6 W. However, it can be loaded up to 12 W. We can generate any value of Q from the assumed heat distribution, by selecting random numbers between 0 and 1, but restricting the maximum value to 12 W. For example, one can select a function as follows,

$$Q_{11} = Q_{avg} + \delta(2 \times \text{rand}(0-1) - 1) \quad (20)$$

Table 2
Comparison of Nusselt numbers and percentage variation with respect to the Nusselt Number for Re = 1500.

Heater	Re = 1500	Re = 3500		Re = 4500	
	Nusselt number	Nusselt number	% Increase with respect to Re, 1500	Nusselt number	% Increase with respect to Re, 1500
1	8.4	12.1	44.0	17.9	112.7
2	11.5	15.3	33.0	24.3	111.2
3	19.5	32.0	64.5	82.3	322.0
4	8.7	13.4	53.8	20.8	138.8
5	10.9	12.9	18.3	21.5	97.2
6	18.6	26.5	42.5	44.3	138.2
7	8.74	14.7	68.2	25.2	188.3
8	17.0	30.3	78.2	26.8	57.6
9	31.2	46.1	48.0	73.2	135.0

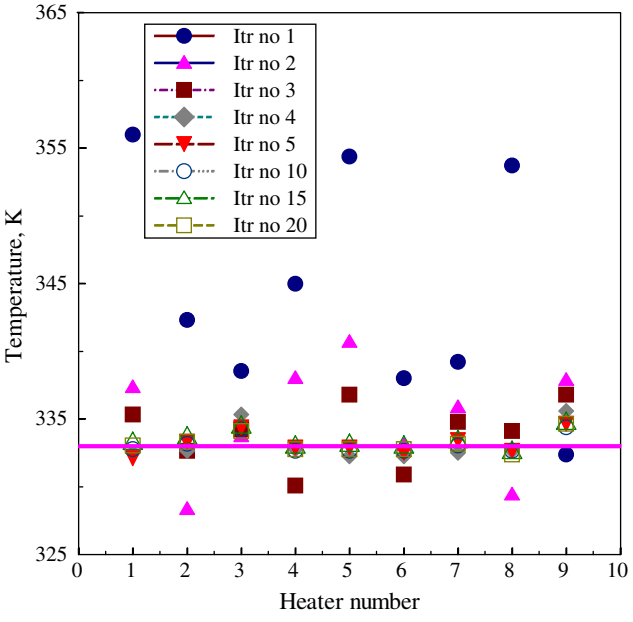

Fig. 11. Plot highlighting the process of convergence of the temperature of various heaters to the target temperature, 333 K.

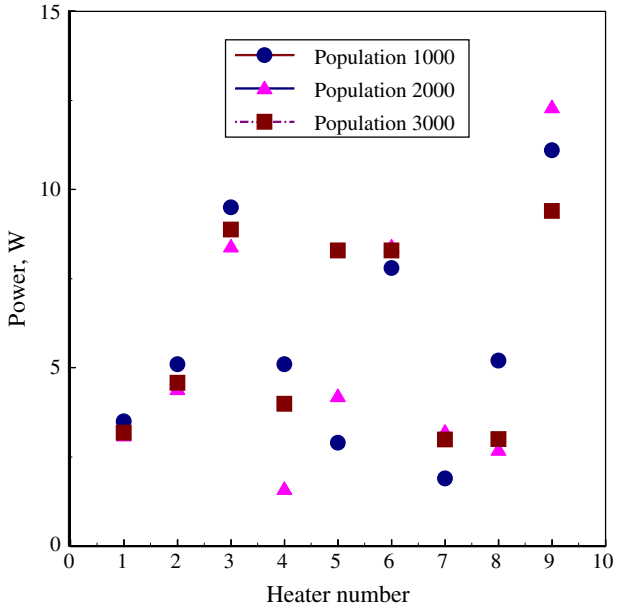

Fig. 12. The power distribution for different populations of selection.

The above function assumes a minimum value of 0 and maximum value of 12 for δ of 6. As the iterations proceed, the value of δ is varied to a low value to minimize the range of the perturbation. Fig. 12 shows the power distribution, upon convergence, for a target temperature 343 K for different populations. It can be noted that for a population of 2000 and 3000, the differences are marginal for most of the heaters and in many cases the optimal heating levels coincide.

Fig. 13 shows the cumulative heat input for different target temperatures. It can be seen that as the target temperature increases, the cumulative heat input of all 9 heaters also increases. The bar chart shown in Fig. 14 depicts the apportioning of the heat input amongst the heaters for different target temperatures. It can be seen that heaters 1, 4 and 7 are loaded to lower values, which are in accordance

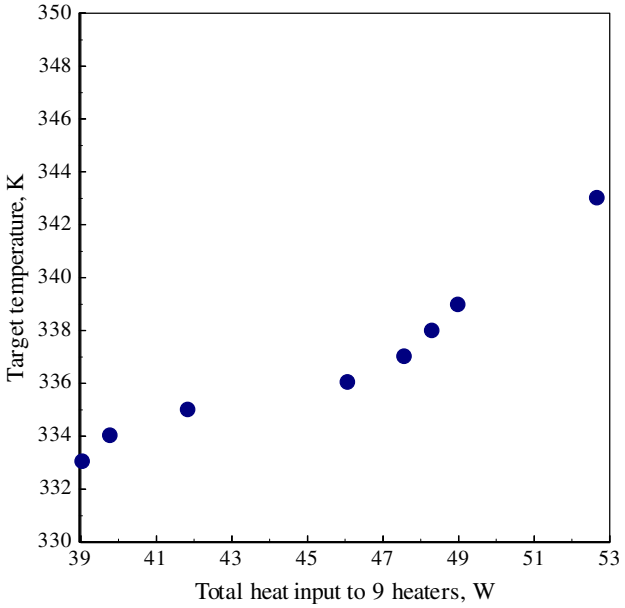

Fig. 13. The total power consumption for different target temperatures.

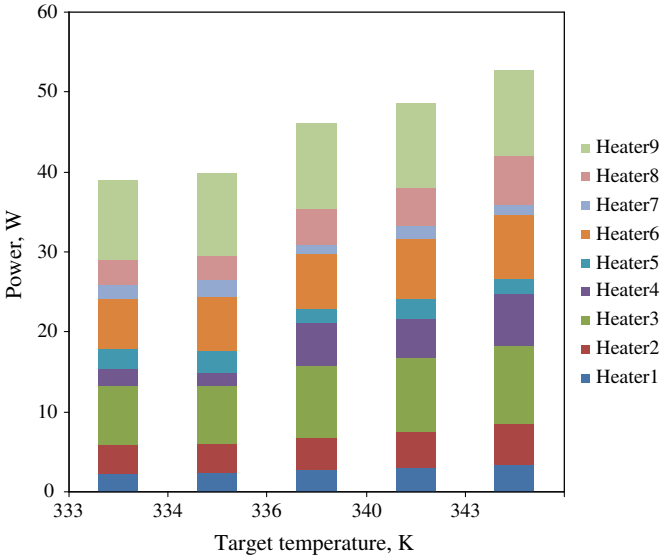

Fig. 14. Bar chart showing the heat distribution for different target temperatures.

with the numerical simulations and the experiments described in previous sections. Heaters 3, 6 and 9 are loaded the most.

5.4.3. Experimental verification

Experiments were carried out to verify the validity of the optima obtained using the procedures outlined in the previous sections. In these experiments, the power distribution to achieve a target temperature of 333 K (from an initial temperature of 303 K, i.e., $\Delta T = 30\ ^\circ C$) is considered. However, during the experimentation the ambient temperature was 27 °C and hence the expected temperature is 330 K. Fig. 15 shows the array of power supply systems and the experimental set up. Table 3 shows a comparison of the experimental and simulated temperatures for the corresponding power inputs. It can be seen that for many heaters, the power input (experimental) agree with the power input (numerical) to within ±2%. The error is mainly due to fact that the number of samples considered for simulations is only 60 and the ambient temperature was slightly different at 27 °C during the experimentation instead of 30 °C chosen as the initial temperature for the numerical simulations. Even though the error in $\sum Q_i$ is 15%, the method adopted clearly indicates that the

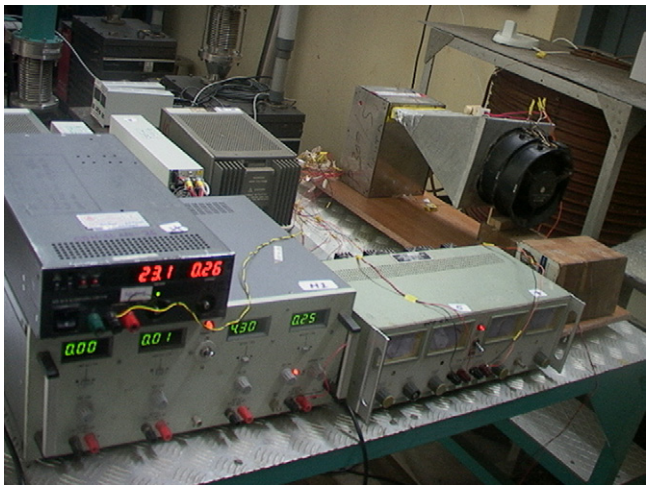

Fig. 15. Experimental arrangement for multiple heater experiments.

Table 3
Comparison of heat input and temperature distribution (numerical) with experimental results.

Heater	Power, W (num)	Temp, K	ΔT (num)	Power, W (expt)	Temp, K	ΔT (expt)	% diff in Temp
1	2.4	333.0	30.22	2.8	328.8	28.8	−1.3
2	3.6	333.0	30.04	4.2	330.7	30.7	−0.70
3	7.7	333.0	30.04	8.0	327.5	27.5	−1.66
4	2.7	333.0	29.92	3.6	329.2	29.2	−1.12
5	2.3	333.0	30	2.5	326.5	26.5	−1.95
6	6.4	333.0	30.03	7.1	329.7	29.7	−1.00
7	1.7	333.0	29.97	2.4	324.4	24.4	−2.57
8	3.3	333.3	30.32	4.2	325.1	25.1	−2.47
9	9.9	333.1	30.14	11.4	328.4	28.4	−1.42
$\sum Q_i$	40.0			46.2			

procedure is quite effective and can be implemented for a general case of "*n*" heaters.

6. Conclusions

In this paper, fluid flow and heat transfer characteristics in a ventilated enclosure, where multiple heaters are arranged in a staggered arrangement have been elucidated. Both experimental and numerical studies have been carried out and the results agree quite well. This was followed by an optimization study to maximize the heat dissipation rate for a given target temperature. Two methods to achieve target temperature for all heaters, namely (i) a trial and error method and (ii) the response surface method were discussed in detail. The latter method was adopted to maximize the heat input and minimize the temperature deviation from a target temperature, simultaneously, by employing a composite objective function. The numerically obtained optimal solution was verified by carrying out experiments. The method of response surface was found to be effective in optimizing the total heat transfer for a given target temperature. The results were also found to be physically meaningful, as it was seen that heaters within the flow can be loaded to a higher level than those placed at other locations. Experimental verification of the optimum validates the numerical procedure.

References

[1] F.C. Lai, F.A. Kulacki, C.Y. Choi, Free and mixed convection in horizontal porous layers with multiple heat sources. AIAA Journal of Thermophysics and Heat Transfer 4 (1990) 221–227.
[2] C.Y. Choi, A. Ortega, Mixed convection in an inclined channel with a discrete heat source, Inter Society Conference on Thermal Phenomena in Electronic Systems, I – THERM – III, (1992) 40–48.
[3] J.N. Funk, M.P. Menguc, K.A. Tagavi, C.J. Cremers, A semi-analytical method to predict printed circuit board package temperatures. Components, Hybrids, and Manufacturing Technology, IEEE Transactions on 15 (1992) 675–684.
[4] T.J. Heindel, F.P. Incropera, S. Ramadhyani, Conjugate natural convection from an array of discrete heat sources: part 2-a numerical parametric study. International Journal of Heat and Fluid Flow 16 (1995) 511–518.
[5] T.C. Hung, S.K. Wang, Fengjee Peter Tsai, Simulations of passivity enhanced conjugate heat transfer across an array of volumetric heat sources. Communications in Numerical Methods in Engineering 13 (1997) 855–866.
[6] S.-Q. Du, E. Bilgen, P. Vasseur, Mixed convection heat transfer in open ended channels with protruding heaters. Heat and Mass Transfer 34 (1998) 263–270.
[7] A.T. Joseph, S.P. Venkateshan, G. Kuruvilla, Experimental studies on cooling of electronic components in a channel. International Journal of Transport Phenomena 3 (2001) 103–118.
[8] Qi-Hong Deng, Guang-Fa Tang, Yuguo Li, Man Yeong Ha, Interaction between discrete heat sources in horizontal natural convection enclosures. International Journal of Heat and Mass Transfer 45 (2002) 5117–5132.
[9] M. Keyhani, R. Cox, V. Prasad, An experimental study of natural convection in a vertical cavity with discrete heat sources. ASME Journal of Heat Transfer (1988) 616–624.
[10] G.I. Sultan, Enhancing forced convection heat transfer from multiple protruding heat sources simulating electronic components in a horizontal channel by passive cooling. Microelectronics Journal 31 (2000) 773–779.
[11] P.J. Rodgers, C. Valérie, Eveloy an experimental assessment of numerical predictive accuracy for electronic component heat transfer in forced convection—Part I: experimental methods and numerical modeling, 125, (2003) 67–75.
[12] P. Rodgers, V. Eveloy, J. Lohan, C.M. Fager, P. Tiilikka, J. Rantala, Experimental validation of numerical heat transfer prediction for single and multi-component printed circuit boards in natural convection environments. Proc., Fifteenth IEEE Semiconductor Thermal Measurement and Management Symposium (SEMI-THERM XV) (1999) 55–64.
[13] S. Baskaya, U. Erturhan, M. Sivrioglu, Experimental investigation of mixed convection from an array of discrete heat sources at the bottom of a horizontal channel. Heat Mass Transfer 42 (2005) 56–63.
[14] Victor M. Perez, John E. Renaud, Adaptive experimental design for construction of response surface approximations. American Institute of Aeronautics and Astronautics, AIAA (2001) 2001–1622.
[15] D. Wang, G.F. Naterer, G. Wang, Adaptive response surface method for thermal optimization: application to aircraft engine cooling system, 8th AIAA/ASME Joint Thermophysics and Heat Transfer Conference, (2002), Missouri, AIAA 2002–3000.
[16] David L. Rodriguez, Response surface based optimization with a Cartesian CFD method, in: 41st Aerospace Science Meeting and Exhibit, (2003). AIAA, Reno, 2003 2003-0465.
[17] Chin-Hsiang Cheng, Hong-Hsiang Lin, Win Aung, Optimal shape design for packaging containing heating elements by inverse heat transfer method. Heat and Mass Transfer 39 (2003) 687–692.
[18] A.K. da Silva, S. Lorente, A. Bejan, Optimal distribution of discrete heat sources on a wall with natural convection. International Journal of Heat and Mass Transfer 47 (2003) 203–214.
[19] Jae-Woo Lee, Kwon-Su Jeon, Yung-Hwan Byun, Sang-Jin Kim, Optimal space launcher design using a refined response surface method. Lecture Notes in Computer Science 3613 (2005) 1081–1091.
[20] Kyoungwoo Park, Seungjae Moon, Optimal design of heat exchangers using the progressive quadratic response surface model. International Journal of Heat and Mass Transfer 48 (2005) 2126–2139.
[21] Kwang-Yong Kim, Ji-Yong Choi, Shape optimization of a dimpled channel to enhance turbulent heat transfer. Numerical Heat Transfer Part A: Applications 48 (2005) 901–915.
[22] Kwang-Yong Kim, Kim Hong-Min, Shape optimization of inclined ribs as heat transfer augmentation device. Journal of Thermal Science 15 (2006) 364–370.
[23] Hsien-Chie Cheng, Yu-Che Huang, Wen-Hwa Chen, A force-directed-based optimization scheme for thermal placement design of MCMSs. IEEE Transactions on Advanced Packaging 30 (2007) 56–67.
[24] Andre I. Khuri, John A. Cornell, Response Surface Design and Analysis, second ed. Marcel Dekker, New York, 1996.
[25] S.J. Kline, F.A. Mcclintock, Describing uncertainties in single sample experiments. Mechanical Engineering 75 (1953) 3–8.